Complete Two-Electron Spectra in Double Photoionization: The Rare Gases Ar, Kr, and Xe

J. H. D. Eland, O. Vieuxmaire, and T. Kinugawa
PTCL, Oxford University, Oxford, United Kingdom

P. Lablanquie
LURE, Centre Universitaire Paris-Sud, 91898 Orsay, France

R. I. Hall and F. Penent
LDIAM, Université Pierre & Marie Curie, 75252 Paris 5, France
(Received 22 September 2002; published 6 February 2003)

A new spectroscopic technique, giving complete two-dimensional e^--e^- coincidence spectra in single photon double photoionization, is presented. The technique resolves the states of doubly charged ions and provides spectra of the individual electrons emitted in formation of each final dication state. Complete spectra for double photoionization of Xe, Kr, and Ar at photon energies up to 51 eV have been recorded. Overall and surprisingly, the $np^4\ ^3P$, ^1D, and ^1S states are populated according to their statistical weights. When the evident autoionization is excluded, the supposedly favored ^3P states are in fact disfavored. Detailed information on the autoionization processes is also made available.

DOI: 10.1103/PhysRevLett.90.053003 PACS numbers: 32.80.Fb, 32.70.Fw

The formation of doubly charged positive ions by single photon ionization is forbidden in the frozen orbital single particle approximation, but occurs widely. Its intensity depends strongly on electron correlation effects and has therefore been intensively studied for many years [1–3]. Even the energy levels of dications have only recently become accurately known through the advent of high resolution techniques, particularly the study of Doppler-free kinetic energy release from molecular double ionization [4,5] and the registration of pairs of zero-energy electrons in coincidence as a function of the photoionizing wavelength [threshold photoelectrons coincidence spectroscopy (TPEsCO) [6,7]]. This last method, which has good resolution and is applicable to atoms and to both bound and dissociative states of molecular dications, is the most powerful technique available hitherto. Its limitation is that the mechanism of production of zero-energy electron pairs is unknown, so the meaning of relative intensities in TPEsCO spectra is uncertain. Furthermore, to measure zero-energy electrons only is to neglect the main bulk of the double photoionization process. The present technique uses all the electrons emitted as pairs in double photoionization, measuring the energy of each. It provides both the spectra of doubly charged ions and the full distributions of electrons forming each state. Double photoionization of Xe, Kr, and Ar at photon energies up to 51 eV has been examined providing new, complete information on this process. It was observed that the $np^4\ ^3P$, ^1D, and ^1S states are populated according to their statistical weights, whereas favored population of the ^3P state was expected. In fact, when the autoionization structure in the electron energy distributions is excluded, the ^3P states are disfavored. The electron energy distributions also furnish information on the autoionization processes revealing selectivity in the decay of some intermediate Xe^+ states to particular Xe^{2+} final states.

The basis of the new technique (Fig. 1) is time-of-flight analysis and coincidence detection of electron pairs in a magnetic bottle after photoionization by pulsed ultraviolet light. A suitable pulsed light source has been developed providing the necessary short ionizing light pulses (ca. 20 ns width) at kHz repetition rates. The lamp combines the hollow cathode effect with a short capillary discharge [8] in helium in a low-inductance coaxial capacitor discharge design. After monochromatization in a toroidal grating instrument and refocusing at a toroidal gold mirror, its light intensity produces count rates of several hundred per second from low pressure ($< 10^{-1}$ mbar) gas targets at 40.8 eV (30.4 nm) photon energy. Lower but useful count rates are available at

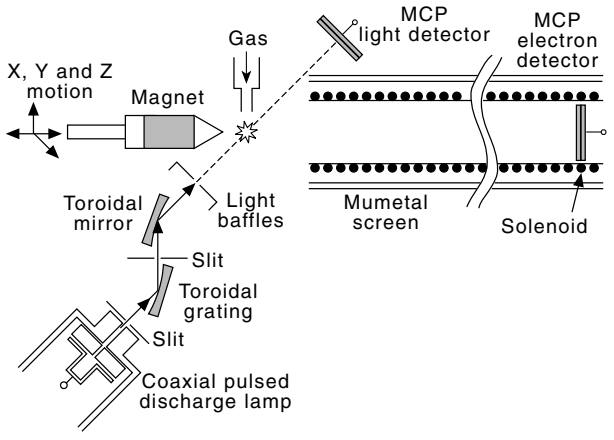

FIG. 1. Scheme of the apparatus. Pumping by turbo molecular pumps at both ends of the flight tube provides a base vacuum of 2×10^{-7} mbar.

 0031-9007/03/90(5)/053003(4)$20.00

38.7 eV (32.0 nm), 48.4 eV (25.6 nm), and 51.0 eV (24.3 nm).

Target gas is supplied as an effusive jet from a 1 mm diameter Cu tube. The magnetic bottle time-of-flight technique spectrometer is based on the original design of Kruit and Read [9] as extended by Cha *et al.* [10] and Wang *et al.* [11], and is 5.5 m long from source to detector. Electrons are guided along the flight path by a solenoidal field of 6×10^{-4} T after parallelization in the inhomogeneous field produced by a 90° conical soft iron pole piece on a cylindrical rare-earth permanent magnet. The divergent field forms a magnetic mirror so that electrons are collected from almost the whole 4π solid angle.

In a magnetic mirror, reflection or loss of electrons created on axis depends only on the angle of emission and not on the electron energy [12]. From the field at our interaction center (0.08 T) and at the pole face (0.23 T), we calculate that over 90% of all electrons should be detectable. By comparing electron pair counts with single electron counts for Xe at 40.8 eV, where the partial cross sections for single and double ionization are known, the overall detection efficiency for electrons is measured as 65%. As this is essentially the efficiency of the multichannel plate detector, the collection efficiency must indeed be near 100%. Its energy independence was verified by measuring single ionization spectra of atoms and small molecules whose corrected photoelectron spectra are known. No systematic deviation from uniform collection efficiency was found up to 35 eV.

The electron energy resolution has been measured using single ionization of rare gas and molecular targets. At high electron energies (> 20 eV), resolution is limited by the light pulse width and is proportional to the $3/2$ power of the energy. At intermediate energies (3–10 eV), it is also limited by the degree of parallelization in the magnetic bottle, proportional to the ratio of magnetic fields in the solenoid and at the source [9]. The measured line width contribution is 1% while the fields indicate 0.7%. At low energies (< 3 eV), an unknown mechanism, possibly electrical patch fields or magnetic field nonadiabaticity, produces a minimum energy width of 40 meV. For double ionization spectra, the accuracy of the energy calibration also affects resolution, because of the wide spread of energies between the two electrons. Calibration lines from molecular spectra and rare gases can be fit precisely to

$$t = t_0 + D/(E + E_0)^{1/2}, \tag{1}$$

with no additional terms.

Of the heavy rare gases, Xe has been most fully studied. We first show the double ionization spectrum of Xe at 40.8 eV. The two-dimensional map in Fig. 2 contains a line for each of the five accessible states of Xe^{2+}; integration along the lines produces the spectrum of Xe^{2+} shown in Fig. 3. The intensity distribution along each line shows how the excess energy is shared between the two outgoing electrons in production of a single final state.

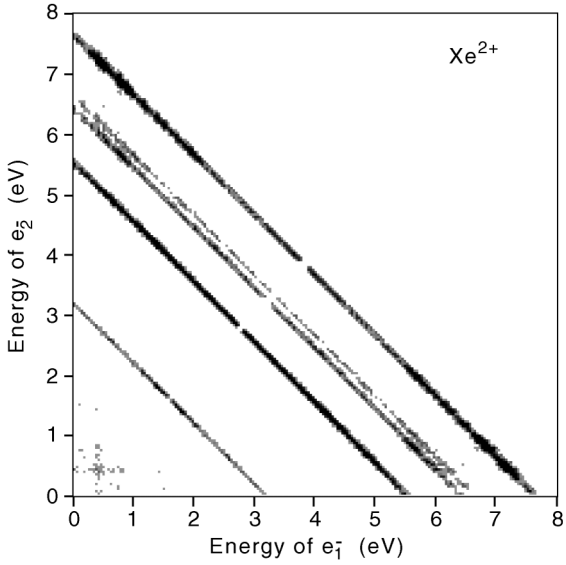

FIG. 2. Complete double photoionization spectrum of Xe at 40.8 eV converted from flight time to energy. Spectrum accumulation times are typically 24 h.

The distributions all run from zero to the maximum electron energy and are symmetrical about half the maximum; at that point a gap appears because electrons of exactly equal flight time are not registered. Any intermediate state of Xe^+ which autoionizes to one of the final Xe^{2+} levels produces two peaks; the first electron is conventionally the photoelectron, and the second, the Auger electron. They can be distinguished because the Auger electron is of the same energy at all wavelengths, while the photoelectron energy varies but its binding energy is always the same. The low-energy half of the distributions for formation of four of the final states on a single electron ionization scale are shown in Fig. 4.

At 40.8 eV, the intensities of the final states $^3P_2$, $^3P_0$, $^3P_1$, ^1D, and ^1S are in proportions 6.5:1.1:2.3:5:0.8. These are close to the statistical weights of 5:1:3:5:1, which is surprising for reasons discussed below. They are somewhat different from the ratios reported from measurements of threshold electron pair yields as a function of photon energy [3,13]. Measurements at other energies (Table I) also give near-statistical total population ratios for the dication states at all photon energies more than a few volts above threshold.

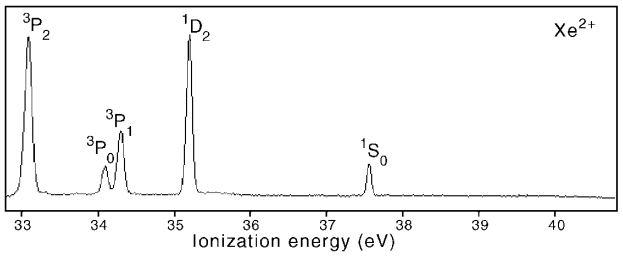

FIG. 3. The spectrum of Xe^{2+} states produced by photoionization at 40.8 eV.

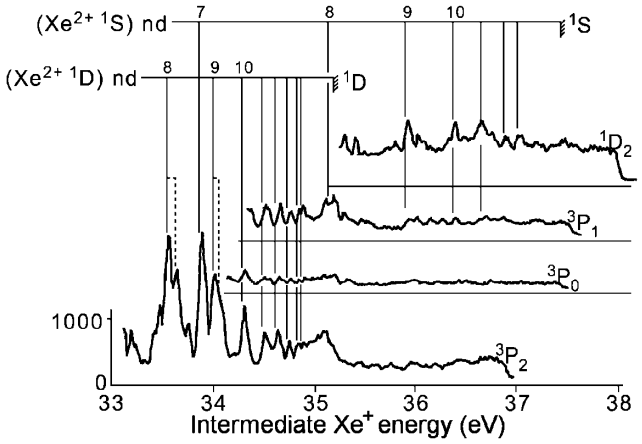

FIG. 4. Spectra of the electrons emitted in photoionization to each of the lowest four states of Xe^{2+}, equivalent to distributions along the lines in Fig. 2 on the e_1^- energy scale. The energy scale is the electron energy plus the formation energy of the Xe^{2+} state indicated and corresponds to the formation energy of Xe^+ states. The zeros are displaced, but a common intensity scale is used for the four spectra.

The spectra of Fig. 4 not only show the existence of autoionization, but also allow estimates of the direct (continuum) and indirect (autoionization) contributions. When the relative areas in the continua are taken, excluding the evident peaks, the intensity ratios at 40.8 eV become 4.6:0.9:1.7:5:0.9 or 7.2:5:0.9 for ^3P, ^1D, and ^1S. Relative continuum intensities at 40.8 eV and other photon energies are given in Table I. The $^3P_2$ and $^3P_0$ levels are populated by electron continuum processes almost exactly in proportion to their statistical weights, but the population of $^3P_1$ seems to be deficient. Using published data for the absorption cross sections [14] and ionization yields [15], Table I can be transformed into partial cross sections at each wavelength for double ionization to each final state, separated into the direct and indirect parts. Only the ^1S states show the expected smooth rise from threshold; the other states have roughly constant or falling partial cross sections at all the measured photon energies, which are some 2 eV and more above the onsets.

Electron distributions for forming the lowest states of Kr^{2+} and Ar^{2+} at 48.4 eV are shown for comparison in Fig. 5. The general features noted for Xe are true of these atoms also; their ^3P states are populated statistically only when autoionization is included.

TABLE I. Xe^{2+} state intensities in photoionization with continuum parts in parentheses.

State (IP)	38.7 eV	40.8 eV	48.4 eV	51.0 eV
$^3P_2$ (33.1 eV)	7.3 (4.9)	6.5 (4.6)	5.9 (4.9)	4.8 (4.3)
$^3P_0$ (34.2 eV)	1.1 (1.2)	1.1 (0.9)	3.9 (3.9)	3.7 (3.9)
$^3P_1$ (34.4 eV)	2.4 (2.3)	2.3 (2.7)		
$^1D_1$ (35.3 eV)	5	5	5	5
$^1S_0$ (37.6 eV)	0.3 (0.3)	0.8 (0.9)	1.6 (1.6)	1.4 (1.7)

The near-statistical population of dication final states in single photon photoionization is quite unexpected. First, if the ionization is mainly direct, the partial cross sections for double ionization should rise approximately linearly from zero at threshold (Wannier law). The lowest final states are the furthest above their respective thresholds, and thus have the largest energy factors in their favor. Second, extended Wannier theory [16,17] states that for reasons of symmetry the ^3P final state, which is the lowest, is the one most favored in direct double ionization near threshold, having no node in the final two-electron wave function at the Wannier point. The other final states have smaller (but nonzero) angular factors in their theoretical cross sections [17]. Third, while direct ionization produces part of the cross section, the spectra show that indirect double ionization (autoionization of Xe^+ intermediate states) also plays a major role, contributing most strongly to the ^3P state. Thus, for three reasons we expect the ^3P state to be most strongly populated. In fact, this level is populated only slightly more than in proportion to its statistical weight when including autoionization, and less if the evident autoionization is not included (Table I). The extended Wannier rules are based on an LS coupling model which is not appropriate for Xe, but in the lighter rare gases, where the LS coupling model should be more valid, the ^3P final state is relatively less populated by continuum double ionization than in Xe. The degree of mixing of the equal-J levels can also be calculated from the level positions [18]; it is never more than 20%, which seems inadequate to explain the observed intensities. The present measurements are perhaps made too far above threshold for the Wannier ideas to apply, but this observation adds no insight to the problem of the observed statistical branching.

In the autoionization spectra in Fig. 4, , Rydberg series of Xe^+ converging on higher Xe^{2+} levels can be identified and $^3P_1$ and ^1S series (not shown) are identified here for the first time. A notable feature is the selectivity of some autoionization branching; states energetically capable of populating either the ^3P levels or ^1D almost all favor ^1D, and some favor individual spin-orbit levels of ^3P. Here, only the contrasting selectivity to branching of the two series shown in Fig. 4 is presented. The series converging to Xe^{2+} (^1D) is known from photoelectron spectra [19,20] and identified as $(^1D)nd(^2S_{1/2})$. The series converging on ^1S has been identified in resonant Auger spectra [21] as $(^1S)nd$. The states of the $(^1D)nd(^2S_{1/2})$ series, which can ionize to all three ^3P levels, do so in accord with the statistical weights of the final levels. On the other hand, the $(^1S)nd$ series shows strong selectivity. The peak identified as $(^1S)9d(^2P)$, for instance, branches as follows: ^1D (18), $^3P_1$ (5), $^3P_0$ (1), $^3P_2$ (not detected), and other members of the same series behave similarly.

According to the selection rules for autoionization [22] and the propensity rules given by Berkowitz [23], purely statistical branching is not expected. For the $(^1D)nd(^2S^e)$

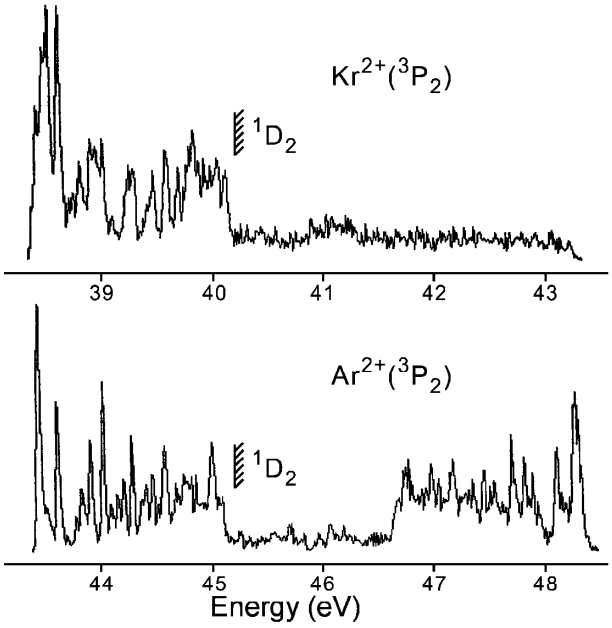

FIG. 5. Spectra showing the electron energy distributions in formation of the $^3P_2$ states of Kr^{2+} and Ar^{2+} at 48.4 eV. The energy scale is the electron energy plus the formation energy of the doubly charged ion state indicated. Note the rather weak continuum contributions. The deterioration of electron energy resolution with increasing energy is clearly seen for Ar where the full, symmetric spectrum is shown.

series of autoionizing states seen in the ^3P channels, the open continua of even parity are $(^3P)\epsilon s$ or $(^3P)\epsilon d$, neither of which has a $^2S^e_{1/2}$ component; thus in strict LS coupling this autoionization is forbidden. This might help explain why the peaks are relatively sharp. If the main autoionization is the favored [23] l-unchanging one, then the Auger electron will be a d wave, but this gives no allowed $\Delta J = 0$ autoionization for the $^3P_0$ level. Thus, the existing rules with the present attribution of the series seem to imply that specificity in branching ought to exist, where in practice none is detected. However, an alternative attribution of the Rydberg series is suggested by another analysis [6,24] of the equivalent series in Ar^+ and Kr^+ as $(^1D)nd(^2D)$. With this attribution, which predicts spin-orbit splitting of the lower series members consistent with our spectra (Fig. 4), no forbidden channels arise.

For the series identified here only as $(^1S)nd$, no restriction is implied by the rules, as continua of overall doublet, even symmetry are available by combining d waves (l-unchanging transition) with the symmetries of all the accessible final dication states. The observed autoionization selectivity must be ascribed to some other cause, perhaps related to the configurationally mixed nature of the states involved, of which the labels applied here may be a very poor representation.

An explanation of these observations may require numerical calculations of the sort recently carried out for higher energy autoionizing states of Ar^+ [25]. The overall conclusion is that our understanding of the processes of double photoionization and of autoionization branching is still unsatisfactory. The widely quoted extended Wannier rules seem to be practically irrelevant for relative cross sections at energies of 5 eV or more above threshold.

[1] V. Schmidt, *Electron Spectrometry of Atoms Using Synchrotron Radiation* (Cambridge University Press, Cambridge, England, 1997).
[2] J. S. Briggs and V. Schmidt, J. Phys. B **33**, R1 (2000).
[3] P. Bolognesi, S. J. Cavanagh, L. Avaldi, R. Camilloni, M. Zitnik, M. Stuhec, and G. King, J. Phys. B **33**, 4723 (2000).
[4] M. Lundqvist, P. Baltzer, D. Edvardsson, L. Karlsson, and B. Wannberg, Phys. Rev. Lett. **75**, 1058 (1995).
[5] S. Hsieh and J. H. D. Eland, J. Phys. B **29**, 5795 (1996).
[6] R. I. Hall, G. Dawber, A. G. McConkey, M. A. MacDonald, and G. C. King, Phys. Rev. Lett. **68**, 2751 (1992).
[7] R. I. Hall, L. Avaldi, G. Dawber, A. G. McConkey, M. A. MacDonald, and G. King, Chem. Phys. **187**, 125 (1994).
[8] P. Choi and M. Favre, Rev. Sci. Instrum. **69**, 3118 (1998).
[9] P. Kruit and F. H. Read, J. Phys. E **16**, 313 (1983).
[10] C. Y. Cha, G. Gantefoer, and W. Eberhardt, Rev. Sci. Instrum. **63**, 5661 (1992).
[11] L. S. Wang, C. F. Ding, X. B. Wang, and S. E. Barlow, Rev. Sci. Instrum. **70**, 1957 (1999).
[12] For example, J. A. Bittencourt, *Fundamentals of Plasma Physics* (Pergamon, New York, 1986), p. 79.
[13] R. I. Hall, G. Dawber, A. G. McConkey, M. A. MacDonald, and G. C. King, Z. Phys. D **23**, 377 (1992).
[14] J. A. R. Samson, Adv. At. Mol. Phys. **2**, 177 (1966).
[15] J. A. R. Samson and G. N. Haddad, Phys. Rev. Lett. **33**, 875 (1974).
[16] C. H. Greene and A. R. P. Rau, J. Phys. B **16**, 99 (1983).
[17] A. Huetz, P. Selles, D. Waymel, and J. Mazeau, J. Phys. B **24**, 1917 (1991).
[18] E. U. Condon and G. H. Shortley, *Theory of Atomic Spectra* (Cambridge University Press, Cambridge, England, 1967), p. 274.
[19] A. Kikas, S. J. Osborne, A. Ausmees, S. Svensson, O. P. Sairanen, and S. Aksela, J. Electron Spectrosc. Relat. Phenom. **77**, 241 (1996).
[20] S. Alitalo, A. Kivimäki, T. Matila, K. Vaarala, H. Aksela, and S. Aksela, J. Electron Spectrosc. Relat. Phenom. **114**, 141 (2001).
[21] G. B. Armen, H. Aksela, T. Aberg, and S. Aksela, J. Phys. B **33**, R49 (2000).
[22] H. G. Kuhn, *Atomic Spectra* (McGraw-Hill, New York, 1992).
[23] J. Berkowitz, *Advances in Chemical Physics* (McGraw-Hill, New York, 1988), Vol. 72, p. 1–36.
[24] M. Hochlaf, H. Kjeldsen, F. Penent, R. I. Hall, P. Lablanquie, M. Lavollée, and J. H. D. Eland, Can. J. Phys. **74**, 856 (1996).
[25] F. Combet-Farnoux, P. Lablanquie, J. Mazeau, and A. Huetz, J. Phys. B **33**, 1597 (2000).